Theoretical Chemistry Accounts (2018) 137:107
https://doi.org/10.1007/s00214-018-2291-3

REGULAR ARTICLE

Keto–enol tautomerism in micro-hydrated acetylacetone: an atoms-in-molecules study

Bastien Casier[1] · Nicolas Sisourat[1] · Stéphane Carniato[1] · Nathalie Capron[1]

Received: 29 January 2018 / Accepted: 2 July 2018 / Published online: 4 July 2018

Abstract
We theoretically investigate the keto–enol tautomerism of micro-hydrated acetylacetone molecule and compare it to the isolated acetylacetone. The minimum energy path was computed through the Climbing-Image Nudged Elastic Band method (CINEB). The density functional theory was applied in the Projector Augmented Wavefunction (PAW) formalism using the generalized gradient approximation within Perdew–Wang (PW91) parametrization. Moreover, a topological and energy partition analysis was done in the framework of the Quantum Theory of Atoms In Molecules (QTAIM). We show that the activation barrier energy decreases from the gas phase to clusters with up to three water molecules surrounding the acetylacetone and increases when four water molecules are considered. Our analysis indicates that the hydrogen bond lattice of the water molecules strongly stabilizes the transition state, leading to the decrease of the activation energy. Furthermore, the size of the proton relay formed by the solvent molecules influences the stretch of the C_α–H bond which explains the increase of the activation energy for the largest cluster.

Keywords DFT · NEB · QTAIM · Micro-hydrated systems · Hydrogen bonds · Tautomerism

1 Introduction

keto–enol tautomerization of β-diketones has been extensively studied in the gas phase [1–14] as well as in protic [13–19] and aprotic solutions [16, 20, 21]. The enol form is generally more stable than the keto one in the gas phase and aprotic solvents while the keto form is dominant in protic solution [16]. Furthermore, in the latter case, the activation barrier energy is significantly lower compared to that in the gas phase, demonstrating an important catalytic effect of the protic solvent molecules [15, 17, 19]. The solvent molecules form a bridge for the proton transmission between the hydrogen atom of the α-carbon and the oxygen atoms of the solute. This appropriate linkage of the solvent cluster and the substrate molecule enhances the proton relays and yields a smaller activation energy [19].

Among these studies, many theoretical works have been reported on keto–enol tautomerization of β-diketones including few explicit solvent molecules [13–15, 17–21] since micro-solvated molecules are important prototypes to bridge the gap between the gas and the condensed phase [22–24]. In Yamabe et al. [19], several β-diketones were investigated with an increasing number of water molecules (from one to six) in several conformations. In general, adding successively more solvent molecules lowers the activation barrier energy. However, in conformations where all water molecules act as a proton relay, a surprising increase of the activation energy was observed from three to four water molecules. To our knowledge, no explanation based on a topological study for such behaviors has been discussed before.

In the present work, we theoretically investigate the keto–enol tautomerization of acetylacetone in the gas phase and in the presence of one to four water molecules forming a proton relay. The decrease of the activation energy from the gas phase to clusters with up to three water molecules and the increase of the activation energy from three to four water molecules are also observed. Using the Quantum Theory of

Electronic supplementary material The online version of this article (https://doi.org/10.1007/s00214-018-2291-3) contains supplementary material, which is available to authorized users.

✉ Bastien Casier
bastien.casier@upmc.fr

[1] Laboratoire de Chimie-Physique, Matière et Rayonnement, CNRS, Sorbonne Université, 75005 Paris, France

Atoms In Molecules (QTAIM), we provide an explanation for such behaviors. Our analysis shed light on the physicochemical properties of water as solvent.

The outline of the article is the following: In Sect. 2, we briefly introduce the methods used in this work. Computational details are given in Sect. 3. Results from our calculations are discussed in Sect. 4. We first compare the activation energies for the acetylacetone in the gas phase and the micro-hydrated molecule. Observed trends are then explained in light of the QTAIM analysis. The article ends with the conclusions of the work.

2 Theoretical background

We studied the tautomerism mechanism involving one, two, three, and four water molecules. All these molecules are bounded by hydrogen bonds and interact with the acetylacetone molecule. Assuming the system follows the minimum energy path (MEP), we optimized the reaction paths of the proton transfer in the framework of the Nudged Elastic Band (NEB) method [25]. Particularly, we used the Climbing-Image NEB (CI-NEB) method developed by Henkelman et al. [26, 27], which is a robust and efficient method to determine the transition state and its geometry. The same method was applied, in our previous work, for the acetylacetone molecule in the gas phase [12]. We then employed a Quantum Theory of Atoms In Molecules (QTAIM) energy partition and a Bond Critical Points (BCPs) analysis to understand the influence and the origin of the effects of the water solvent molecules.

2.1 The energy partition

In the QTAIM, an atomic basin Ω is defined as a region of real space bounded by surfaces through which there is a zero flux in the gradient vector field of the electron density [28]. The atomic energy is defined as the sum of a kinetic ($\mathcal{T}_{\text{el}}$) and a potential ($\mathcal{V}$) contribution:

$$E_{\text{at}}^{\Omega} = \mathcal{T}_{\text{el}}(\Omega) + \mathcal{V}(\Omega),$$

these two energetic quantities are linked through the virial theorem, such as

$$-2\mathcal{T}_{\text{el}}(\Omega) = \mathcal{V}(\Omega). \tag{1}$$

The potential part gathers the electron–electron ($\mathcal{V}_{\text{el-el}}$), electron–nuclear ($\mathcal{V}_{\text{el-nu}}$), and nuclear–nuclear ($\mathcal{V}_{\text{nu-nu}}$) interactions, as

$$\mathcal{V}(\Omega) = \mathcal{V}_{\text{el-el}}(\Omega) + \mathcal{V}_{\text{el-nu}}(\Omega) + \mathcal{V}_{\text{nu-nu}}(\Omega) + \mathcal{V}_{\text{ext}}(\Omega),$$

and $\mathcal{V}_{\text{ext}}$ corresponds to the virial of the external forces acting on the nuclei and results from the Hellmann–Feynman [29] theorem.

Hence, two ways can be used to compute the atomic energy, and we calculate either the virial potential part or the virial kinetic part. Nevertheless, the virial potential part is determined with difficulty for large systems, mainly because a good definition of the atomic basins is needed and the electronic density requires to be correctly defined on a fine grid of points [30]. Therefore, this way is really time-consuming and it is more efficient to use the virial kinetic part [31–33].

From the works of Bader et al. [31, 32], it is possible to define two local kinetic energy distribution functions

$$\mathcal{K}(\mathbf{r}) = -\frac{1}{2}\sum_i \lambda_i \left[\phi_i(\mathbf{r})\nabla^2\phi_i(\mathbf{r})\right] \tag{2}$$

and

$$\mathcal{G}(\mathbf{r}) = \frac{1}{2}\sum_i \lambda_i \left[\nabla\phi_i(\mathbf{r})\cdot\nabla\phi_i(\mathbf{r})\right], \tag{3}$$

where the ϕ_i's are the natural orbitals and λ_i's their occupation numbers. Moreover, these two definitions are locally gauged by the Laplacian ($\mathcal{L}(\mathbf{r})$), such that

$$-\frac{1}{4}\mathcal{L}(\mathbf{r}) = \mathcal{K}(\mathbf{r}) - \mathcal{G}(\mathbf{r}).$$

The two kinetic forms integrated in a correct atomic volume Ω must be the same, and the Laplacian thus equals zero. Hence, the Laplacian plays an important role in the control of the integration convergence. In our calculations, the Laplacian integrated in each atomic basin was smaller than 10^{-4} a.u.

Finally, from virial theorem Eq. (1) and from the definition of two kinetic functions Eqs. (2) and (3), we have for the atomic energy

$$E_{\text{at}}^{\Omega} = -\mathcal{T}_{\text{el}}(\Omega) = -\mathcal{K}(\Omega) = -\mathcal{G}(\Omega).$$

with

$$\mathcal{K}(\Omega) = \int_{\Omega}\mathcal{K}(\mathbf{r})\mathrm{d}\mathbf{r}, \qquad \mathcal{G}(\Omega) = \int_{\Omega}\mathcal{G}(\mathbf{r})\mathrm{d}\mathbf{r}$$

2.2 Energy decomposition scheme

From the previous definition of the atomic energy, we define some molecular basins $\mathcal{G}$ as groups of atoms Ω. We can recover the total energy of the system through the sum over all groups:

$$E = \sum_{\mathcal{G}}\left(\sum_{\Omega\in\mathcal{G}} E_{\text{at}}^{\Omega}\right).$$

Blanco et al. [34] define, from these groups of atoms, two kinds of energies. The first is the net energy of the molecular basin ($E_{\text{net}}^{\mathcal{G}}$) and the second the interaction between groups ($E_{\text{int}}^{\mathcal{GH}}$). The total energy can be recovered as:

$$E = \sum_{\mathcal{G}} E^{\mathcal{G}}_{\text{net}} + \frac{1}{2} \sum_{\mathcal{G}} \sum_{\mathcal{G} \neq \mathcal{H}} E^{\mathcal{G}\mathcal{H}}_{\text{int}}.$$

The net energy of each group is obtained by a simple energy point calculation for the isolated molecular group maintained in the geometry of the full system. Then, the interaction energy is just the difference between the total energy partitioned by the QTAIM in the two molecular basins and their associated net energy:

$$E^{\mathcal{G}}_{\text{int}} = \left(\sum_{\Omega \in \mathcal{G}} E^{\Omega}_{\text{at}} \right) - E^{\mathcal{G}}_{\text{net}}$$

In the following, we are interested in two groups of atoms: the acetylacetone molecule ($\mathcal{G}$ = ACAC) and the water cluster ($\mathcal{G}$ = Water). Furthermore, we used the net ($E^{\mathcal{G}}_{\text{net}}$) and the interaction energy ($E^{\mathcal{G}}_{\text{int}}$) of each molecular basin $\mathcal{G}$ to investigate the role played by the water proton relay on the activation energy of the keto–enol tautomerization.

2.3 The bond critical points (BCP)

Further insights are obtained by analyzing the electronic density. For any geometry, a particular electronic density characterized by a large set of stationary points (extrema and saddle points) is obtained. The nature and the position of these points reflect the attractive and repulsive forces in presence. We focused in this work on the BCPs (indicated by $\mathbf{r}_{\text{bcp}}$ in the following). These BCPs allow us to construct the *molecular graph* of the different studied systems. It is an unambiguous representation of the interactions and can thus be used to locate changes in the structure along the reaction path [28].

In fact, the local properties of the BCPs enable to determine the nature of the bond. A covalent bond presents a negative value of the Laplacian $\nabla^2\rho(\mathbf{r}_{\text{bcp}})$, which refers to a charge accumulation. Inversely, a non-covalent bond is specified by a positive Laplacian [35]. In the latter case, there is a depletion in the charge around the bonding region which induces a closed-shell bonding. It is the case of hydrogen bonds or van der Waals interactions [36]. The nature of a bond can be further analyzed with the local energy density $\mathcal{H}(\mathbf{r}_{\text{bcp}})$. This energy density was introduced by Cremer and Kraka [37] and defined as

$$\mathcal{H}(\mathbf{r}) = \mathcal{G}(\mathbf{r}) + \mathcal{V}(\mathbf{r}).$$

It is a powerful topological criterion to estimate precisely the nature and the strength of the bond [38]. Grabowski et al. [39] brought an important systematization in the description of the three types of interactions through the local Laplacian and the energy density: A bond can be covalent, non-covalent, or partially covalent according to the criteria given in Table 1.

Despite these properties which are not often used in QTAIM studies, we show in this work that they provide a greater understanding of the modifications occurring into the molecular graph around the transition-state region. In particular, the energy density appears to be a relevant property to understand the origin of the energy variations in each molecular basin.

3 Computational details

To study the influence of the size of the water cluster onto the activation barrier, we used the CI-NEB method with different numbers of explicit water molecules through the proton path (**1w**, **2w**, **3w**, and **4w**). For each cluster size, we have chosen a stable conformer in which all water molecules are involved in the proton relay. The geometries of these conformers are similar to those investigated in the work of Yamabe et al. [19] in the case of the malondialdehyde.

Initially, the NEB method was implemented for condensed matter studies. Nevertheless, this method can be applied efficiently to the gas phase too [12, 40]. Hence, the reaction paths and the associated transition states (saddle points) were determined through the VASP code [41, 42] using the CI-NEB method [26, 27]. The Density Functional Theory (DFT) in the Projected Augmented Wave [43] (PAW) formalism was used, employing a Generalized Gradient Approximation (GGA) functional with Perdew–Wang [44] (PW91) parameters. It should be noted that entropic effects are neglected here: At room temperature, these corrections change the energy barrier by about 5% [13]. We therefore only considered electronic energies in our study.

As the VASP code applies periodic boundary conditions, the convergence of the electronic energy with respect to the box size has been checked. Consequently, each system was considered isolated inside a sufficiently big unit cell and the unique Γ point was used to compute the electronic energy. Several periodic codes rely on the use of plane wave basis set. It is not common to study a single molecule from this wavefunction expansion. However, for large systems, and particularly when hydrogen bonds are involved in the cluster, the plane waves appear to be advantageous [45, 46]. It should also be mentioned that other ab initio molecular dynamics and electronic calculations of isolated molecules were performed in the framework of plane waves basis sets [47–49].

Finally, in order to compare our NEB activation energies obtained by VASP/PW91 with previous results from the

Table 1 Grabowski's criteria for the nature of the bonds [39]

Covalent (**C**)	$\nabla^2\rho(\mathbf{r}_{\text{bcp}}) < 0$	$\mathcal{H}(\mathbf{r}_{\text{bcp}}) < 0$
Partially covalent (**PC**)	$\nabla^2\rho(\mathbf{r}_{\text{bcp}}) > 0$	$\mathcal{H}(\mathbf{r}_{\text{bcp}}) < 0$
Non-covalent (**NC**)	$\nabla^2\rho(\mathbf{r}_{\text{bcp}}) > 0$	$\mathcal{H}(\mathbf{r}_{\text{bcp}}) > 0$

literature [15, 17], we performed, from the NEB geometries of the activated complexes, B3LYP/6-31G(d) calculations using Gaussian03 [50].

We checked that the energy gradient is null and that one imaginary frequency is obtained at the transition state (TS) for each cluster size. For one and two water molecule(s) included in the unit cell, a small number of intermediate geometries between the initial (β-diketone) and the final state (enolone) were sufficient to describe the MEP and to obtain the transition state (TS) with the CI-NEB method. However, for three and four water molecules, this number of intermediate geometries had to be increased to obtain the TS. The number of images used for each CI-NEB calculation is given in Table 2.

A QTAIM analysis from a calculation based on a pseudopotential is possible but remains difficult for some bonds. For example, no bond critical point was found between oxygen and hydrogen atoms (O–H) when a pseudopotential was employed. As shown in the work of Yim and Klüner [30], it is essential to include the core electrons contribution into the electronic density. Therefore, we computed the wavefunctions for the initial and the transition states from G03/PW91/6-311++G** calculations with Gaussian03 [50]. Finally, our partition of the total electronic energy was done through the PROAIM code [51] within the AIMPAC suite of programs from the Mc Master University.

4 Results and discussion

We first present the results of the NEB calculations with different sets of explicit solvatation water molecules involved in the proton transfer. The activation energies and the TS geometries are reported and discussed. Furthermore, we analyze the changes of the activation energies for the systems with different number of water molecules in light of the QTAIM energy partition. In a second part, a BCPs analysis of the systems at the TS which provides insights in the tautomerism mechanism is given.

4.1 NEB results

Using the CI-NEB method, the MEP was determined for one (**1w**), two (**2w**), three (**3w**), and four (**4w**) water molecules. In the initial diketo configurations, the water molecules form a bridge between the central carbon atom (C1) and the oxygen atom (O1) of a ketone function and hence constitute a proton relay for the tautomerization (see Fig. 1). Figure 2 shows the evolution of the activation barrier as function of the number of water molecules into the proton relay. (Activation energies as well as the energy differences ($\Delta E_{Enol\text{-}Keto}$) are given in Online Resource Table 9.)

In vacuum, where the proton transfer is direct from β-diketone to enolone form, the reaction barrier is very high with 49.41 kcal/mol [12]. The inclusion in the proton path of water molecules involves a diminution of the activation energy which reveals the catalytic role played by the solvent molecules. The barrier falls from 49.41 to 19.82 kcal/mol (**1w**), 10.89 kcal/mol (**2w**), and 9.92 kcal/mol (**3w**) for one, two, and three molecules in the cluster, respectively. In the case of four solvent molecules, the activation energy rises up to 12.03 kcal/mol (**4w**). This tendency was already mentioned by Yamabe et al. [19] for another β-diketone, the malondialdehyde molecule. Our results confirm that a proton relay with three solvent molecules is therefore optimal for the tautomerization.

In order to compare our NEB transition states obtained from the VASP/PW91 calculations with data from the literature, we computed the energies at the obtained TS geometries with another level of theory G03/B3LYP/6-31G(d) (see Fig. 2 and Table 9 in Online Resource). Our energies differ by less than 10% with those of the literature results [15, 17]; therefore, our NEB geometries match well with these previous calculations. We can underline that the PW91 values are slightly smaller than the B3LYP ones. This difference in the energies can be explained by the way in which the hydrogen bond is described in these two functionals. In fact, Tsuzuki et al. [52] have shown, on a large set of hydrogen-bonded complexes, that the interaction energies calculated by PW91 are better described than with the B3LYP functional [52]. Their results have shown that the performance of the B3LYP depends on the Becke exchange functional which is not efficient in the space regions where the electronic density is low as for hydrogen bonds. In the next section, we analyze the activation energy for the micro-hydrated acetylacetone molecule using the QTAIM energy partition and BCPs analysis. To apply onto the electronic density a correct QTAIM analysis, we computed the wavefunction through G03/PW91/6-311++G** calculations. The energies obtained with the two basis sets differ by less than 20%. The G03/PW91/6-311++G** energies are slightly higher. The differences are attributed to the size of the basis set, according to the work of Fellers et al. [45].

4.2 Energy partition

We focus in the following on the acetylacetone molecule surrounded by the water molecules. The aim is to explain the general decrease of the activation energy with increasing number of solvent molecules and the surprising increase for four water molecules.

Table 2 Number of images used for each CI-NEB calculation presented in this work

Number of water molecules	**1w**	**2w**	**3w**	**4w**
NEB chain	6	8	16	18

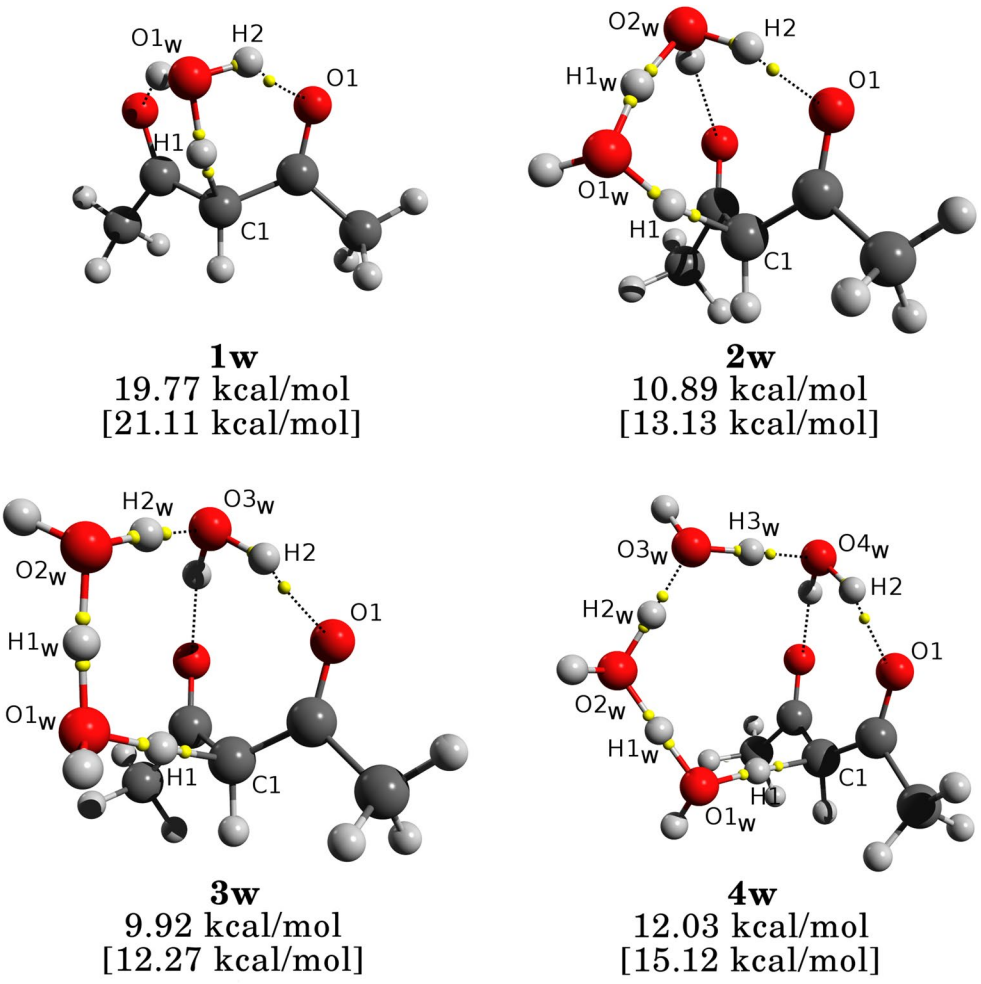

Fig. 1 Transition-state geometries for the four studied systems. The activation energies computed with VASP/PW91 are given without brackets, and the G03/PW91/6-311++G** energies are given between square brackets. The yellow dots show the position of the BCPs involved into the proton transfer (the properties of these BCPs are given in Online Resource Tables 10 and 11)

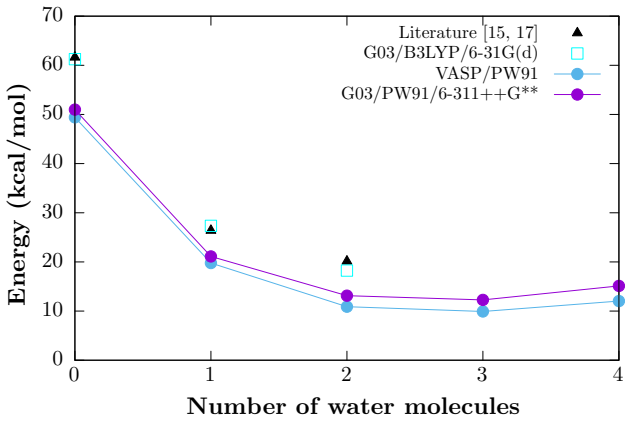

Fig. 2 Activation energies as a function of the number of water molecules (with respect to the energy of the diketo forms)

The total activation energy ($\Delta E^{\ddagger} = E_{TS} - E_{Keto}$) for each system was partitioned into contribution from the water subsystem ($\Delta E^{\ddagger\,Water} = E_{TS}^{Water} - E_{Keto}^{Water}$) and from the acetylacetone molecule ($\Delta E^{\ddagger\,ACAC} = E_{TS}^{ACAC} - E_{Keto}^{ACAC}$). Figure 3a shows the different contributions. The activation energy of the ACAC molecule rises as the number of surrounding water molecules increases. Conversely, the activation energy of the water molecules is negative and decreases from one to four water molecules. Therefore, the decrease of the total activation energy is provided by the water relay. Furthermore, the increase of the total activation energy which appears for four water molecules is due to the large elevation energy occurring in the β-diketone. This energy increase is not counterbalanced by the energy decrease induced by the water cluster.

To go further, we split the activation energy into the total net and interaction energies as well as the contributions of each subgroup. Net and interaction parts of the activation energy are shown in Fig. 3b, c, respectively. The comparison between the two figures shows that the total interaction part is negative and responsible for the decrease of the total activation energy. Furthermore, it is shown in Fig. 3c that the interaction part of the water subsystems decreases faster than that of the ACAC molecule increases. Therefore, the total activation energy decreases from one to three water molecules because the ACAC

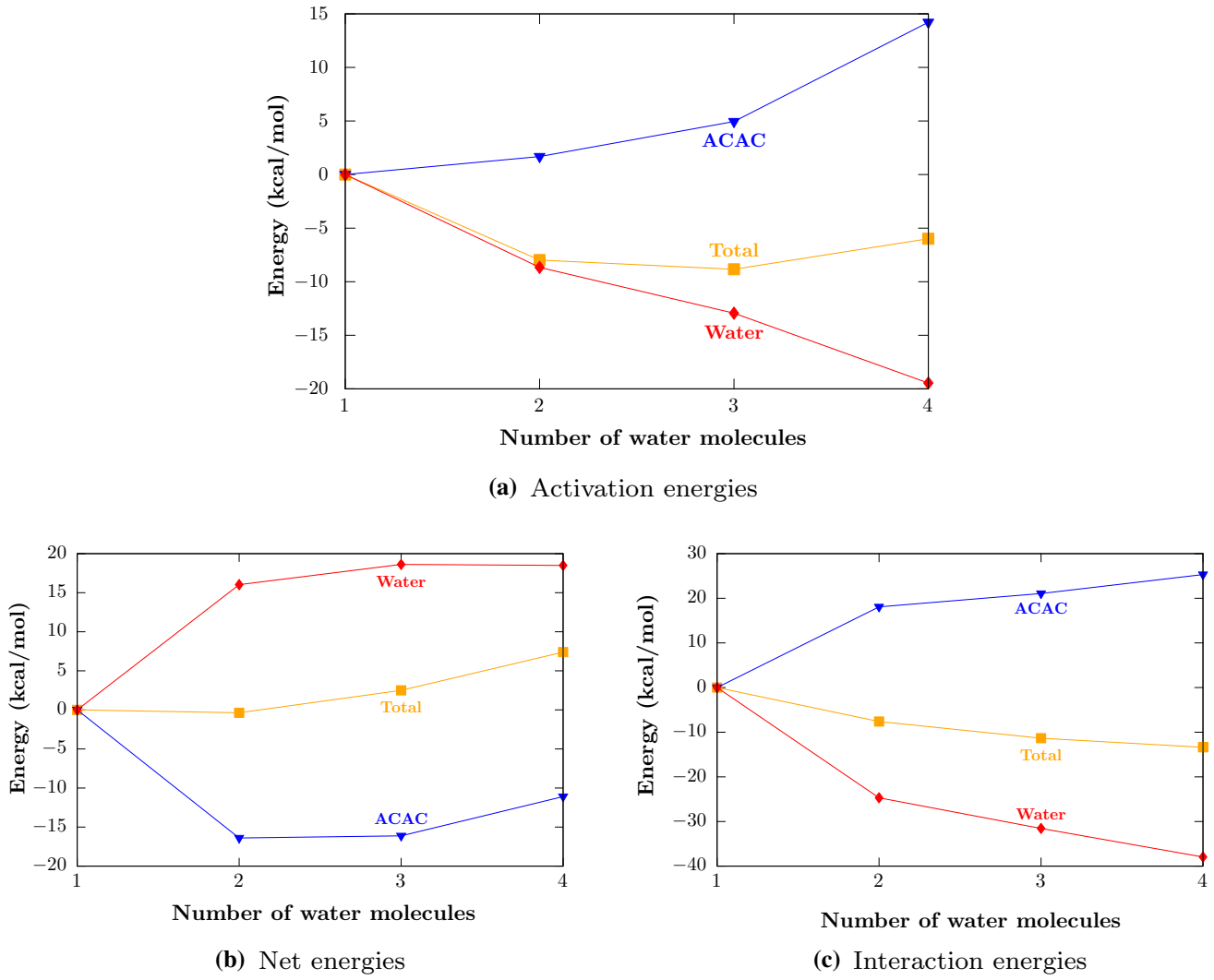

Fig. 3 Activation energy and the two energy contributions (net and interaction) of the subsystems as a function of the number of water molecules. The values are from Table 3 where the first values were shifted to zero

molecule stabilizes more the water network than the latter destabilizes the ACAC molecule. Conversely, the rise in the activation energy from three to four water molecules comes from the net contribution of the ACAC molecule. On the one hand, as shown in Fig. 3b, the ACAC molecule is stabilized for two and three water molecules and is disturbed when the water cluster size is increased to four. On the other hand, the net energy of the water cluster first increases from one to three and then remains nearly constant.

The QTAIM energy partition allowed us to pinpoint which subsystem and which part of the energy are responsible for the changes in the total activation energy. Based on this analysis, we can go further and get greater insights by analyzing some relevant BCPs at the TS geometries.

4.3 BCPs analysis

The nature, according to the Grabowski's criteria [39], of some relevant bonds at the initial and TS geometries is given in Online Resource Tables 10 and 11, respectively. The BCPs analysis revealed that no covalent bonds are broken at the transition states despite a strong stretch of the C1–H1 bond. Moreover, we can underline that at the TS geometry a H–O covalent bond is created between the hydrogen atom (H1), which leaves the central carbon, and the oxygen atom ($O1_w$) of the closest water molecule. This H1-$O1_w$ interaction, as shown by the initial state BCPs (see Online Resource Table 10), was initially non-covalent. It should also be noted that the alcohol function (H2–O1) is not formed at the transition state for these systems. Indeed,

Table 3 Contributions of the activation energies

Number of water molecules	1w	2w	3w	4w
Activation energy				
$\Delta E^{\ddagger}$ (kcal/mol)	20.49	13.51	12.50	15.24
$\Delta E^{\ddagger\,\mathrm{ACAC}}$ (kcal/mol)	39.38	41.06	44.33	53.59
$\Delta E^{\ddagger\,\mathrm{Water}}$ (kcal/mol)	−18.89	−27.55	−31.83	−38.35
Net energy				
$\Delta E^{\ddagger}_{\mathrm{net}}$ (kcal/mol)	46.16	45.79	48.66	53.55
$\Delta E^{\ddagger\,\mathrm{ACAC}}_{\mathrm{net}}$ (kcal/mol)	41.73	25.33	25.61	30.63
$\Delta E^{\ddagger\,\mathrm{Water}}_{\mathrm{net}}$ (kcal/mol)	4.43	20.46	23.05	22.92
Interaction energy				
$\Delta E^{\ddagger}_{\mathrm{int}}$ (kcal/mol)	−25.67	−32.28	−36.16	−38.31
$\Delta E^{\ddagger\,\mathrm{ACAC}}_{\mathrm{int}}$ (kcal/mol)	−2.35	15.73	18.72	22.96
$\Delta E^{\ddagger\,\mathrm{Water}}_{\mathrm{int}}$ (kcal/mol)	−23.32	−48.01	−54.88	−61.27

Note that the sum of the activation energies ($\Delta E^{\ddagger\,\mathrm{ACAC}}$ and $\Delta E^{\ddagger\,\mathrm{Water}}$) does not give exactly the total activation energy. The small difference comes from the numerical integration of the energies in the different atomic basins [51]

the H2–O1 bond keeps its non-covalent nature. However, the energy density becomes negative which shows that the bond is strengthened.

This general analysis shows that the C1–H1 bond is the most disturbed bond of the ACAC molecule. Furthermore, the covalent bonds of the water clusters are not significantly perturbed. In the following, we thus focus on the C1–H1 bond of the ACAC molecule and the hydrogen bond lattice of the water clusters.

We first discuss the behavior of the interaction energy since it is responsible for the decrease of the total activation energy for water cluster size from one to three. To understand the behavior of the interaction energies into the activation energy, we compared the energy densities of the BCPs of the water cluster and of the β-diketone, each kept isolated, with the energy densities of BCPs when these entities interact. Table 4 shows the variation of the energy densities of the C1–H1 bond and of the hydrogen bonds between the initial diketo and the TS geometries. The difference of the energy densities was computed with ($\Delta\mathcal{H}^{\ddagger}$) and without ($\Delta\mathcal{H}^{\ddagger}_{\mathrm{net}}$) including the other system. It is shown that the variation of the energy density of the C1–H1 bond is more positive in the full system than for the isolated ACAC molecule. Hence, the water cluster disturbs this bond, mainly from the new covalent bond established between H1 and $O1_w$. This may explain the increase of the interaction energy of the ACAC molecule. Inversely, the water cluster subsystem is stabilized by the interactions. Indeed, the hydrogen bonds ($H1_w$-$O1_w$, $H2_w$–$O2_w$, and $H3_w$–$O4_w$) are reinforced by the ACAC molecule due to a more negative variation of the energy densities. The consequence is the contraction of the hydrogen bond lattice [38], leading to a decrease in the interaction

Table 4 Comparisons of the energy density variations at the transition state between the case with interaction ($\Delta\mathcal{H}^{\ddagger}$) and the case without ($\Delta\mathcal{H}^{\ddagger}_{\mathrm{net}}$) for the C1–H1 bond and the hydrogen bonds

Number of water molecules	1w	2w	3w	4w
Energy density C1–H1				
$\Delta\mathcal{H}^{\ddagger}_{\mathrm{net}}$ (10^{-1} a.u.)	1.89	1.64	1.71	1.82
$\Delta\mathcal{H}^{\ddagger}$ (10^{-1} a.u.)	1.96	1.74	1.89	2.01
Energy density $H1_w$–$O2_w$				
$\Delta\mathcal{H}^{\ddagger}_{\mathrm{net}}$ (10^{-2} a.u.)		−8.02	−9.84	−10.9
$\Delta\mathcal{H}^{\ddagger}$ (10^{-2} a.u.)		−9.19	−10.9	−12.0
Energy density $H2_w$–$O3_w$				
$\Delta\mathcal{H}^{\ddagger}_{\mathrm{net}}$ (10^{-2} a.u.)			−5.58	−5.48
$\Delta\mathcal{H}^{\ddagger}$ (10^{-2} a.u.)			−6.16	−5.85
Energy density $H3_w$–$O4_w$				
$\Delta\mathcal{H}^{\ddagger}_{\mathrm{net}}$ (10^{-2} a.u.)				−3.80
$\Delta\mathcal{H}^{\ddagger}$ (10^{-2} a.u.)				−4.17

energy of the water clusters. The interactions play therefore a very important role in the reaction. First, the water cluster through the $H1$–$O1_w$ bond activates the C1–H1 bond by weakening it; thus, the interaction energy in the ACAC basin increases and disturbs this subsystem. Second, into the water system, the hydrogen bonds are reinforced by the interactions with the ACAC molecule and stabilize the cluster.

We now explain the increase of the total activation energy from three to four water molecules. The previous energy partition analysis indicated that the reason is to be found in the net energy of the ACAC molecule. We therefore focus on the C1–H1 bond. The variation of the energy density between the initial and the transition state at the C1–H1 bond (see Table 4) is less positive for two and three water molecules compared to one and four molecules. As a consequence of it, the stretching of the C1–H1 bond is shorter for the former cases compared to latter ones. These results show that a proton relay with two and three water molecules allows to keep the ACAC molecule at the TS in a geometry close to the diketo one, leading to a low activation energy. Conversely, for one and four solvent molecules, a proton transfer between the ACAC molecule and the water cluster is partially achieved at the TS which induces a higher activation barrier.

In the following, we compare the results of our analysis to those of previous studies. We first discuss the case of one to three water molecules compared to the gas phase. In Yamabe et al. [19], the decrease of the activation energy is explained by a less strained proton relay when the water molecules are included. Our analysis partially agrees with this interpretation: The net activation energy in the ACAC molecule decreases in the presence of the water molecules, which reveals that the conformation of the ACAC molecule, in interaction with the water cluster, is less constrained than

in vacuum. The water molecules open the four-membered ring and keep the solute in a geometry close to its initial state. Hence, according to the Hammonds postulate, this leads to a decrease of the activation barrier.

However, our results show that the interaction energy plays an important role in the diminution of the activation barrier. As shown in Table 4, all the hydrogen bonds involved in the water cluster are reinforced at the transition state. We think it is due to a cooperative effect induced by the interactions with the ACAC molecule. The cooperativity of hydrogen bonds has been observed in several micro-solvated systems [22, 53, 54]. The effect is induced by a modification of the hydrogen bonds environment—particularly through their donor–acceptor character—and can strengthen (cooperative effect) or weaken (anticooperative effect) these bonds [55]. For example, Pérez et al. [22] have experimentally and theoretically investigated the propiolactone molecule micro-solvated with two and three water molecules (note that the geometry of their clusters is close to ours). Through a Natural Bond Orbital (NBO) analysis, they have shown the same effect in their minimal energy conformation [22]—i.e., reinforcement of the hydrogen bonds. In our study, we show that this effect is more pronounced at the transition state.

The increase of the activation barrier with four water molecules has only been observed by Yamabe et al. [19] for the malondialdehyde molecule. These authors explain this behavior by the fact that the size of the relay network is too large to afford the cis enol form of an intramolecular hydrogen bond. In the case of the ACAC molecule with four water molecules, we obtained a TS for which the cis enol form of an intramolecular hydrogen bond is possible. The rise of the energy barrier instead comes from a partial proton transfer of the C_α at the TS geometry.

5 Conclusion

In conclusion, we have investigated the mechanism of the keto–enol tautomerization in micro-hydrated acetylacetone molecule using the Nudged Elastic Band method and the Quantum Theory of Atoms In Molecules. The minimum energy paths were determined for the isolated molecule and for clusters containing up to four water molecules. Our results show that the activation barrier energy decreases from zero to three water molecules surrounding the acetylacetone and increases when four water molecules are considered. Our results confirm that a three-water proton relay is optimal for the keto–enol tautomerism reaction of β-diketone molecules, as already noted by Yamabe et al. [19] in the case of malondialdehyde molecule. Furthermore, our analysis based on energy partition and bond critical points provides the first explanation for such behaviors: The lowering of the barrier energy is due to a strong stabilization of the hydrogen bond lattice of the water network while the peculiar increase for four water molecules comes from a significant stretch of the C_α–H bond.

References

1. Bauer SH, Wilcox CF (1997) On malonaldehyde and acetylacetone: are theory and experiment compatible? Chem Phys Lett 279:122–128
2. Belova NV, Sliznev VV, Oberhammer H, Girichev GV (2010) Tautomeric and conformational properties of β-diketones. J Mol Struct 978:282–293
3. Belova NV, Oberhammer H, Trang NH, Girichev GV (2014) Tautomeric properties and gas-phase structure of acetylacetone. J Org Chem 79:5412–5419
4. Buemi G, Zuccarello F (1997) Importance of steric effect on the hydrogen bond strength of malondialdehyde and acetylacetone 3-substituted derivatives: an ab initio study. Electron J Theor Chem 2:302–314
5. Camerman A, Mastropaolo D, Camerman N (1983) Molecular structure of acetylacetone: a crystallographic determination. J Am Chem Soc 105:1584–1586
6. Caminati W, Grabow JU (2006) The C2 $_v$ structure of enolic acetylacetone. J Am Chem Soc 128:854–857
7. Egan W, Gunnarsson G, Bull TE, Forsen S (1977) A nuclear magnetic resonance study of the intramolecular hydrogen bond in acetylacetone. J Am Chem Soc 99:4568–4572
8. Folkendt MM, Weiss-Lopez BE, Chauvel JP, True NS (1985) Gas-phase proton NMR studies of keto-enol tautomerism of acetylacetone, methyl acetoacetate, and ethyl acetoacetate. J Phys Chem 89:3347–3352
9. Sliznev VV, Lapshina SB, Girichev GV (2006) Ab initio study of the structure of enolic and ketonic forms of β-diketones. J Struct Chem 47:220–231
10. Lowrey AH, George C, D'Antonio P, Karle J (1971) Structure of acetylacetone by electron diffraction. J Am Chem Soc 93:6399–6403
11. Srinivasan R, Feenstra JS, Park ST, Xu S, Zewail AH (2004) Direct determination of hydrogen-bonded structures in resonant and tautomeric reactions using ultrafast electron diffraction. J Am Chem Soc 126:2266–2267
12. Capron N, Casier B, Sisourat N, Piancastelli MN, Simon M, Carniato S (2015) Probing keto-enol tautomerism using photoelectron spectroscopy. Phys Chem Chem Phys 17:19991–19996
13. Alagona G, Ghio C (2008) Keto-enol tautomerism in linear and cyclic β-diketones: a DFT study in vacuo and in solution. Int J Quantum Chem 108:1840–1855
14. Nagy PI, Alagona G, Ghio C (2007) Theoretical investigation of tautomeric equilibria for isonicotinic acid, 4-pyridone, and acetylacetone in vacuo and in solution. J Chem Theory Comput 3:1249–1266
15. Kaweetirawatt T, Yamaguchi T, Higashiyama T, Sumimoto M, Hori K (2012) Theoretical study of ketoenol tautomerism by quantum mechanical calculations. J Phys Org Chem 25:1097–1104
16. Spencer JN, Holmboe ES, Kirshenbaum MR, Firth DW, Pinto PB (1982) Solvent effects on the tautomeric equilibrium of 2, 4 -pentanedione. Can J Chem 60:1178–1182
17. Alagona G, Ghio C, Nagy PI (2010) The catalytic effect of water on the keto-enol tautomerism: a computational challenge. Phys Chem Chem Phys 12:10173–10188

18. Schlund S, Baslio Janke EM, Weisz K, Engels B (2010) Predicting the tautomeric equilibrium of acetylacetone in solution: the right answer for the wrong reason? J Comput Chem 31:665–670
19. Yamabe S, Tsuchida N, Miyajima K (2004) Reaction paths of keto-enol tautomerization of β-diketones. J Phys Chem A 108:2750–2757
20. Delchev VB (2004) Hydrogen bonded complexes of acetylacetone and methanol: HF and DFT level study. Monatsh Chem 135:249–260
21. Delchev VB, Mikosch H (2005) H-bonded complexes between acetylacetone and two molecules of methanol: HF and DFT level study. J Mol Model 11:474–480
22. Pérez C, Neill JL, Muckle MT, Zaleski DP, Peña I, Lopez JC, Alonso JL, Pate BH (2015) Water-water and Water-Solute interactions in microsolvated organic complexes. Angew Chem Int Ed 54:979–982
23. Postulka J, Slavicek P, Fedor J, Farnik M, Kocisek J (2017) Energy transfer in microhydrated Uracil, 5-Fluorouracil, and 5-Bromouracil. J Phys Chem B 121:8965–8974
24. Geyer P, Sezer U, Rodewald J, Mairhofer L, Dörre N, Haslinger P, Eibenberger S, Brand C, Arndt M (2016) Perspectives for quantum interference with biomolecules and biomolecular clusters. Phys Scr 91:063007
25. Jònsson H, Mills G, Jacobsen KW (1998) Classical and quantum dynamics in condensed phase systems. World Scientific, Singapore, pp 385–404
26. Henkelman G, Uberuaga BP, Jònsson H (2000) A climbing image nudged elastic band method for finding saddle points and minimum energy paths. J Chem Phys 113:9901–9904
27. Henkelman G, Jònsson H (2000) Improved tangent estimate in the nudged elastic band method for finding minimum energy paths and saddle points. J Chem Phys 113:9978–9985
28. Matta C, Boyd RJ (2007) The quantum theory of atoms in molecules. Wiley-VCH Verlag GmbH, New York, pp 1–34
29. Feynman RP (1939) Forces in molecules. Phys Rev 56:340–343
30. Yim WL, Klüner T (2008) Atoms-in-molecules analysis for plane-wave DFT calculations: a numerical approach on a successively interpolated charge density grid. J Comput Chem 29:1306–1315
31. Bader RFW, Beddall PM (1972) Virial field relationship for molecular charge distributions and the spatial partitioning of molecular properties. J Chem Phys 56:3320–3329
32. Bader RFW, Beddall PM (1973) Virial partitioning of charge distributions and properties of diatomic hydrides. J Am Chem Soc 95:305–315
33. Bader RFW, Beddall PM (1973) Theoretical development of a virial relationship for spatially defined fragments of molecular systems. J Chem Phys 58:557–566
34. Blanco MA, Martín Pendás A, Francisco E (2005) Interacting quantum atoms: a correlated energy decomposition scheme based on the quantum theory of atoms-in-molecules. J Chem Theory Comput 1:1096–1109
35. Zheng S, Meng L, Cai X, Xu Z, Fu X (1997) Topological studies on IRC paths of X+H2→XH+H reactions. J Comput Chem 18:1167–1174
36. Koch U, Popelier PLA (1995) Characterization of C–H–O hydrogen bonds on the basis of the charge density. J Phys Chem 99:9747–9754
37. Cremer D, Kraka E (1984) Chemical bonds without bonding electron density does the difference electron-density analysis suffice for a description of the chemical bond ? Angew Chem Int Ed Engl 23:627–628
38. Espinosa E, Molins E, Lecomte C (1998) Hydrogen bond strengths revealed by topological analyses of experimentally observed electron densities. Chem Phys Lett 285:170–173
39. Grabowski SJ, Sokalski WA, Dyguda E, Leszczyski J (2006) Quantitative classification of covalent and noncovalent H-bonds. J Phys Chem B 110:6444–6446
40. González-García N, Pu J, González-Lafont A, Lluch JM, Truhlar DG (2006) Searching for saddle points by using the nudged elastic band method: an implementation for gas-phase systems. J Chem Theory Comput 2:895–904
41. Kresse G, Hafner J (1993) Ab initio molecular dynamics for liquid metals. Phys Rev B Condens Matter Mater Phys 47:558–561
42. Kresse G, Furthmüller J (1996) Efficient iterative schemes for ab initio total-energy calculations using a plane-wave basis set. Phys Rev B Condens Matter Mater Phys 54:11169–11186
43. Blöchl PE (1994) Projector augmented-wave method. Phys Rev B Condens Matter Mater Phys 50:17953–17979
44. Perdew JP, Chevary JA, Vosko SH, Jackson KA, Pederson MR, Singh DJ, Fiolhais C (1992) Atoms, molecules, solids, and surfaces: applications of the generalized gradient approximation for exchange and correlation. Phys Rev B Condens Matter Mater Phys 46:6671–6687
45. Fellers RS, Barsky D, Gygi F, Colvin M (1999) An ab initio study of DNA base pair hydrogen bonding: a comparison of plane-wave versus Gaussian-type function methods. Chem Phys Lett 312:548–555
46. Kruse H, Goerigk L, Grimme S (2012) Why the standard B3LYP/6-31G* model chemistry should not be used in DFT calculations of molecular thermochemistry: understanding and correcting the problem. J Org Chem 77:10824–10834
47. Jenkins SJ, King DA (2000) Pentaprismane and hypostrophene from first-principles, with plane waves. Chem Phys Lett 317:381–387
48. Cucinotta CS, Ruini A, Catellani A, Stirling A (2006) Ab Initio molecular dynamics study of the ketoenol tautomerism of acetone in solution. ChemPhysChem 7:1229–1234
49. Kaschner R, Hohl D (1998) Density functional theory and biomolecules: a study of glycine, alanine, and their oligopeptides. J Phys Chem A 102:5111–5116
50. Frisch MJ, Trucks GW, Schlegel HB, Scuseria GE, Robb MA, Cheeseman JR, Montgomery Jr JA, Vreven T, Kudin KN, Burant JC, Millam JM, Iyengar SS, Tomasi J, Barone V, Mennucci B, Cossi M, Scalmani G, Rega N, Petersson GA, Nakatsuji H, Hada M, Ehara M, Toyota K, Fukuda R, Hasegawa J, Ishida M, Nakajima T, Honda Y, Kitao O, Nakai H, Klene M, Li X, Knox JE, Hratchian HP, Cross JB, Bakken V, Adamo C, Jaramillo J, Gomperts R, Stratmann RE, Yazyev O, Austin AJ, Cammi R, Pomelli C, Ochterski JW, Ayala PY, Morokuma K, Voth GA, Salvador P, Dannenberg JJ, Zakrzewski VG, Dapprich S, Daniels AD, Strain MC, Farkas O, Malick DK, Rabuck AD, Raghavachari K, Foresman JB, Ortiz JV, Cui Q, Baboul AG, Clifford S, Cioslowski J, Stefanov BB, Liu G, Liashenko A, Piskorz P, Komaromi I, Martin RL, Fox DJ, Keith T, Al-Laham MA, Peng CY, Nanayakkara A, Challacombe M, Gill PMW, Johnson B, Chen W, Wong MW, Gonzalez C, Pople JA (2004) Gaussian 03, Revision C.02, Gaussian, Inc., Wallingford, CT
51. Biegler-König FW, Bader RFW, Tang TH (1982) Calculation of the average properties of atoms in molecules. J Comput Chem 3:317–328
52. Tsuzuki S, Lüthi HP (2001) Interaction energies of van der Waals and hydrogen bonded systems calculated using density functional theory: assessing the PW91 model. J Chem Phys 114:3949–3957
53. Wu XP, Wei XG, Sun XM, Ren Y, Wong NB, Li WK (2010) Theoretical study on the role of cooperative solvent molecules in the neutral hydrolysis of ketene. Theor Chem Acc 127:493–506
54. Kabanda MM, Tran VT, Tran QT, Ebenso EE (2014) A computational study of pyrazinamide: tautomerism, acid-base

properties, micro-solvation effects and acid hydrolysis mechanism. Comput Theor Chem 1046:30–41
55. Guevara-Vela JM, Romero-Montalvo E, Gómez VAM, Chávez-Calvillo R, García-Revilla M, Francisco E, Pendás AM, Rocha-Rinza T (2016) Hydrogen bond cooperativity and anticooperativity within the water hexamer. Phys Chem Chem Phys 18:19557–19566